JOURNAL OF MATERIALS SCIENCE 28 (1993) 5269–5274

Processing maps for hot working of Cu–Ni–Zn alloys

Part I α-*nickel silver*

D. PADMAVARDHANI, Y. V. R. K. PRASAD
Department of Metallurgy, Indian Institute of Science, Bangalore 560 012, India

The constitutive behaviour of α-nickel silver in the temperature range 700–950 °C and strain rate range 0.001–100 s^{-1} was characterized with the help of a processing map generated on the basis of the principles of the "dynamic materials model" of Prasad *et al.* Using the flow stress data, processing maps showing the variation of the efficiency of power dissipation (given by $2m/(m+1)$ where m is the strain-rate sensitivity) with temperature and strain rate were obtained. α-nickel silver exhibits a single domain at temperatures greater than 750 °C and at strain rates lower than 1 s^{-1}, with a maximum efficiency of 38% occurring at about 950 °C and at a strain rate of 0.1 s^{-1}. In the domain the material undergoes dynamic recrystallization (DRX). On the basis of a model, it is shown that the DRX is controlled by the rate of interface formation (nucleation) which depends on the diffusion-controlled process of thermal recovery by climb. At high strain rates (10 and 100 s^{-1}) the material undergoes microstructural instabilities, the manifestations of which are in the form of adiabatic shear bands and strain markings.

1. Introduction

The constitutive behaviour of materials under hot deformation is influenced significantly by the alloying additions. For example, the dynamic recrystallization (DRX) process in aluminium is promoted by the addition of magnesium or zinc [1] whereas in steels DRX is related by increasing carbon content [2]. It was shown [3] that with increasing solute content, the onset of DRX of austenite is delayed and the rate of recrystallization decreased in plain carbon steels. The influence of alloying additions on the hot deformation characteristics was reviewed by McQueen and Jonas [4] and Sherby and Burke [5]. The evolution of DRX in Cu and Cu–Zn alloys has been studied [6, 7] as a function of zinc content. It was shown [7] that the DRX in these alloys is controlled by diffusion-dependent climb. The addition of 4–9% Mn to two-phase Cu–Ni–Zn alloys was reported to improve the workability [8].

The aim of the present investigation is to study the processing response of α-Cu–Zn alloy to the addition of nickel, which increases the activation energy for diffusion [9]. As the DRX in Cu–Zn alloys is dependent on diffusion-controlled climb, a change in the DRX characteristics is expected with the addition of nickel. This study will also be helpful in understanding the hot deformation behaviour of α–β nickel silver since it is shown that in the hot deformation of two-phase Cu–Zn alloys, α is the controlling factor [10]. Therefore a change in the constitutive behaviour of the α phase is expected to cause a corresponding change in the constitutive behaviour of the α–β alloy. In the present study, the approach of characterizing the hot deformation behaviour using processing maps has been adopted. The basis for this approach is the "dynamic materials model" (DMM) developed by Prasad *et al.* [11] and reviewed recently by Gegel *et al.* [12] and Alexander [13]. This model was used recently to establish processing maps for the hot working of zirconium [14], aluminium [15] and 70:30 brass [16]. Although α-nickel silvers have good cold workability, their hot workability is poor. The hot workability is impaired by impurities like lead and bismuth [17]. The addition of Mischmetall was shown to improve the hot ductility of impure and deliberately leaded nickel silvers which were homogenized at 670 °C [17].

2. The dynamic materials model

The model is applicable to high-temperature deformation where the workpiece essentially acts as a dissipator of power. The constitutive equation describes the manner in which the power is converted at any instant into two forms: thermal and microstructural, which are not recoverable by the system. The dissipator element can be considered to be non-linear, dynamic and irreversible. At any instant, the total power dissipated consists of two complementary parts: G, the content representing the temperature increase and J, the co-content representing the dissipation occurring through metallurgical processes. The factor that partitions power between G and J is the strain rate sensitivity m of flow stress and the J co-content given by [11]

$$J = \sigma\dot{\varepsilon}m/(m+1) \quad (1)$$

0022–2461

where σ is flow stress and $\dot{\varepsilon}$ is strain rate. For an ideal linear dissipator, $m = 1$ and $J = J_{max} = \sigma\dot{\varepsilon}/2$. The efficiency of power dissipation of a non-linear dissipator may be expressed as a dimensionless parameter:

$$\eta = J/J_{max} = 2m/(m+1) \quad (2)$$

The variation of η with temperature and strain rate represents the characteristics of power dissipation through microstructural changes in the workpiece material.

The power dissipation maps are continuum maps but the domains may be interpreted in terms of specific atomistic processes. This can be done with the help of Raj maps [18]. In hot deformation there are "safe" and "damage" mechanisms that occur in different strain-rate–temperature regimes. For example, the safe mechanisms involve dynamic recovery and dynamic recrystallization while the damage mechanisms are wedge cracking (dominant at the lower strain rates and higher temperatures) and void formation at hard particles (dominant at higher strain rates and lower temperatures). The damage processes are generally highly efficient in dissipating energy through production of new surfaces, while the safe processes are relatively less efficient since power dissipation occurs by annihilation of dislocations or their groups. In the safe regime, dynamic recrystallization is more efficient than dynamic recovery.

3. Experimental procedure

Alpha-nickel silver with 25.6% Zn, 12.3% Ni and balance Cu was used in the study. The material was taken in the as-cast condition and was tested in the temperature range 700–950 °C and strain-rate range 0.001–100 s^{-1}.

Cylindrical specimens of 10 mm diameter and 15 mm height were used for the compression testing of the alloys. Care was taken to obtain closely parallel load-bearing surfaces for the specimen. Grooves were provided on these surfaces so that effective lubrication was ensured during compression. Borosilicate glass was used as the lubricant. The temperature of the specimen was monitored with the help of a Chromel–Alumel thermocouple embedded in a 0.8 mm hole machined at half the height of the specimen. This thermocouple was also used for measurement of the adiabatic temperature rise in the specimen during deformation. A computer-controlled servohydraulic testing machine (Dartec, UK) was used for conducting the hot compression tests. This machine was equipped with an exponential decay of the actuator speed so that constant true strain rates in the range 0.0003–100 s^{-1} could be imposed on the specimen. Isothermal tests were conducted by surrounding the specimen, platens and push-rods by a three-zone furnace. The temperature was controlled within ± 2 °C. The adiabatic temperature rise was recorded with the help of a Nicolet transient recorder. In each case, the specimens were compressed to about half their height. The deformed specimens were water-quenched and examined using standard metallographic techniques.

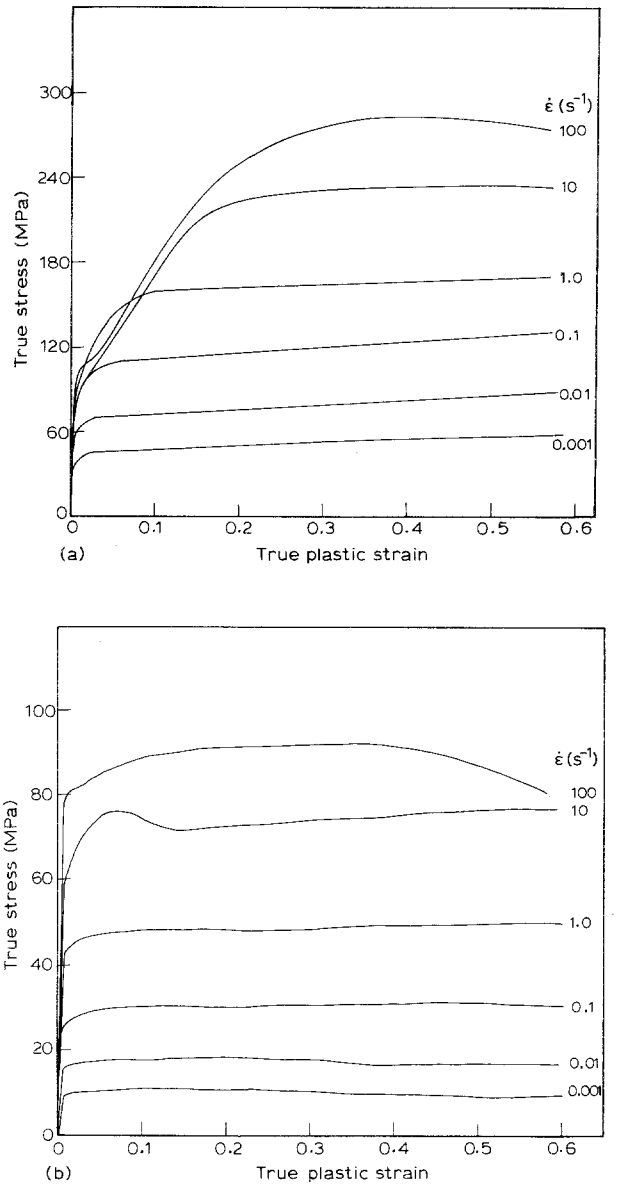

Figure 1 (a) True stress–true plastic strain curves for α-nickel silver at (a) 700 °C and (b) 950 °C and at various strain rates.

4. Results

4.1. Stress–strain curves

Typical true stress–true plastic strain curves recorded on α-nickel silver are shown in Fig. 1a and b for temperatures 700 and 950 °C, respectively, and different strain rates. The following features are observed:

1. At 700 °C, at strain rates lower than 1 s^{-1} steady-state stress–strain curves were observed whereas at higher strain rates hardening occurred at initial strains.
2. At 950 °C, at strain rates lower than 1 s^{-1} slight flow softening followed by a steady state is observed. At higher strain rates oscillations are seen.

The flow stress data corrected for the adiabatic temperature rise are shown in Table I for α-nickel silver.

4.2. Processing maps

The processing map of α-nickel silver is shown in Fig. 2 for a strain of 0.5. The maps obtained at lower

TABLE I Flow stress values of α-nickel silver at different strain rates and temperatures for various strains (corrected for adiabatic temperature rise)

Strain	Strain rate (s^{-1})	Flow stress (MPa)					
		700 °C	750 °C	800 °C	850 °C	900 °C	950 °C
0.1	0.001	47.1	37.7	25.5	18.4	16.1	11.1
	0.01	72.4	57.4	41.6	31.2	25.0	18.5
	0.1	118.5	86.2	66.5	46.6	32.3	29.9
	1	178.2	135.1	107.8	78.6	61.4	48.8
	10	167.2	168.0	157.3	121.6	95.1	76.0
	100	165.6	187.8	185.7	142.4	118.4	94.1
0.2	0.001	49.5	40.5	27.1	19.7	15.3	10.0
	0.01	75.0	59.9	44.4	31.6	26.1	18.7
	0.1	121.9	89.0	70.4	46.7	32.9	29.9
	1	185.8	138.6	110.1	78.4	62.6	48.7
	10	259.5	195.3	159.9	121.4	94.9	74.8
	100	257.8	242.1	208.4	150.7	126.7	96.9
0·3	0.001	52.9	42.9	26.1	19.2	14.9	9.6
	0.01	78.4	62.3	45.9	31.7	25.9	17.3
	0.1	126.1	91.5	73.2	46.8	33.4	30.6
	1	186.3	141.9	113.4	78.7	63.8	49.5
	10	271.8	201.9	163.0	121.9	96.5	76.4
	100	297.5	261.4	218.6	155.1	130.3	98.0
0.4	0.001	55.2	44.6	26.0	19.6	14.2	9.5
	0.01	82.5	64.9	46.7	31.9	25.5	17.0
	0.1	130.5	95.0	76.4	48.0	33.9	30.5
	1	188.0	144.8	116.9	79.8	65.6	50.1
	10	273.0	203.6	165.4	125.7	98.0	77.1
	100	306.7	268.3	222.8	155.9	131.8	98.2
0.5	0.001	57.0	45.7	25.9	20.0	13.7	9.5
	0.01	85.6	67.0	46.8	31.9	24.9	16.6
	0.1	134.5	98.1	78.2	48.7	34.6	30.4
	1	189.1	146.7	118.5	80.8	66.4	50.3
	10	264.9	206.8	167.6	126.8	98.9	78.8
	100	306.6	265.2	220.6	152.9	129.4	93.6

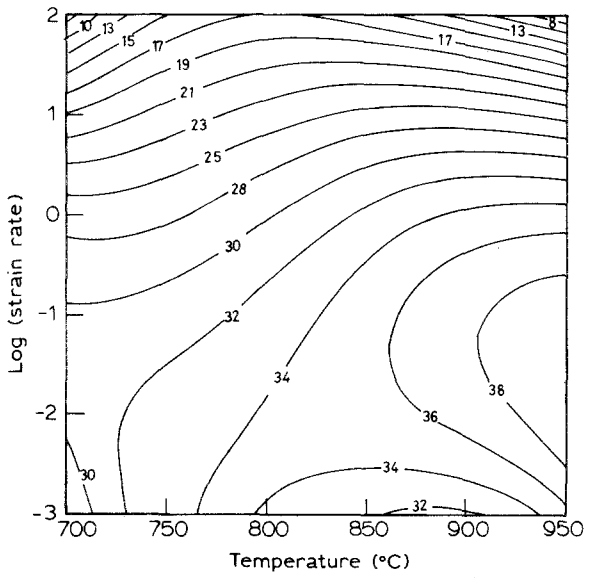

Figure 2 Contour map showing iso-efficiency contours in strain rate–temperature plane for α-nickel silver at a strain of 0.5. The numbers indicate the percentage efficiency of power dissipation.

strains are essentially similar to Fig. 2. The map exhibits a single domain at strain rates lower than 1 s^{-1} and at temperatures greater than 750 °C, with a maximum efficiency of power dissipation of 38% occurring at about 950 °C and 0.1 s^{-1}. In comparison with the map for α-brass [16] wherein a maximum efficiency of 53% was observed at 850 °C, the maximum efficiency in the present case is only 38%. Also, the strain rate for the peak efficiency has gone up by two orders of magnitude (from 0.001 s^{-1} in the map of α-brass to 0.1 s^{-1} in the case of α-nickel silver).

4.3. Instability maps

The regimes of microstructural instabilities are evaluated using the criterion developed by Kumar [19] and Prasad [20]. The criterion was developed on the basis of continuum principles as applied to large plastic flow, proposed by Ziegler [21], according to which instability occurs when

$$\frac{dD}{d\dot{\varepsilon}} < \frac{D}{\dot{\varepsilon}} \tag{3}$$

where D is the dissipation function at a given temperature and $\dot{\varepsilon}$ is the effective strain rate. According to the dynamic materials model [11], D is equivalent to J co-content ($J = \sigma\dot{\varepsilon}m/(m+1)$, σ being the flow stress) which represents the power dissipation through microstructural changes and hence Equation 3 becomes

$$\frac{\partial[\ln(m/(m+1)]}{\partial(\ln\dot{\varepsilon})} + m < 0 \tag{4}$$

The left-hand side of Equation 4 is denoted by $\xi(\dot{\varepsilon})$ which when negative, causes microstructural instability in the material.

The $\xi(\dot{\varepsilon})$ variation as a function of strain rate and temperature is evaluated and represented as an instability map in Fig. 3, for a strain of 0.5. The instability maps for other strains are also similar to this. Curve H is the lower limit for the occurrence of instability which dominates at higher strain rates. The instability map may be superimposed on the power dissipation map (Fig. 2) to delineate the regime of unstable flow.

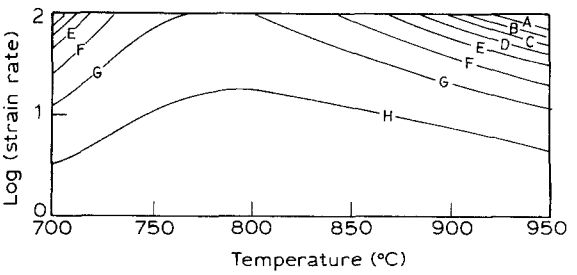

Figure 3 Instability map showing contours of instability parameter $\xi(\dot{\varepsilon})$ in strain rate–temperature plane for α-nickel silver at a strain of 0.5. Instability is predicted when $\xi(\dot{\varepsilon})$ is negative. Values of $\xi(\dot{\varepsilon})$ are as follows: (A) −0.88, (B) −0.75, (C) −0.63, (D) −0.50, (E) −0.38, (F) −0.25, (G) −0.13, (H) 0.00.

5. Discussion

5.1. Domain of dynamic recrystallization

The processing maps are interpreted in terms of microstructural mechanisms using Raj maps [18]. On this basis, any domain at temperatures greater than $0.75T_m$ and at intermediate strain rates may be interpreted in general to represent the process of DRX. This interpretation was confirmed in α-brasses recently [7, 16, 22] on the basis of the matching forgeability–efficiency, tensile elongation–efficiency variations and the sigmoidal variation of the grain size with temperature across the domain (similar to that observed in static recrystallization). In Fig. 4 the variations of the efficiency and the average grain diameter with temperature are shown for α-nickel silver. The grain size variation with temperature is sigmoidal in nature. Also, there is similarity in the trends of the efficiency and grain size variations as a function of temperature. Therefore, the domain under consideration represents the process of DRX. The observed stress–strain behaviour, namely flow softening reaching a steady state with increasing strain, is typical of DRX in low-stacking fault energy materials [23] and is consistent with this interpretation.

The initial microstructure is shown in Fig. 5a and a typical DRX structure in Fig. 5b, which corresponds to a specimen deformed at 950 °C and 0.01 s^{-1} (conditions within the domain corresponding to the efficiency peak). The initial microstructure is typical of cast structure showing very large grains, while the DRX microstructure is characterized by waviness of grain boundaries. Similar features were also observed in α-brass [16, 22].

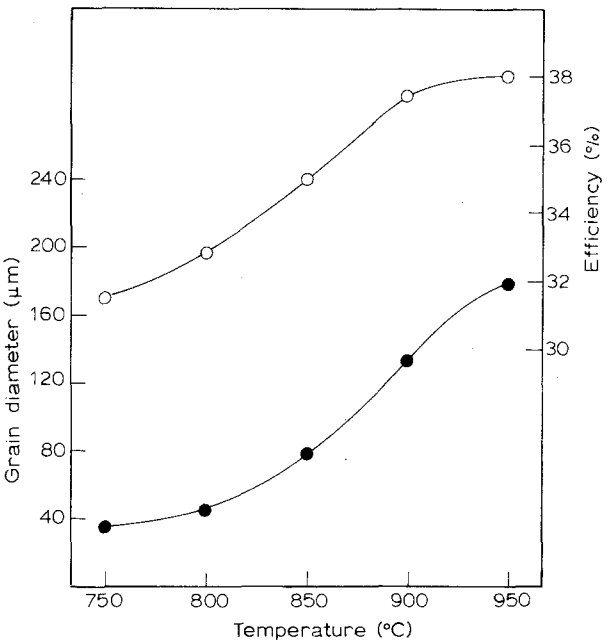

Figure 4 Variation with temperature of (●) average grain diameter and (○) efficiency of power dissipation of α-nickel silver.

5.2. Mechanism of dynamic recrystallization

The results are explained on the basis of a model by Ravichandran and Prasad [24]. According to the model, DRX may be considered to consist of two competing processes–formation of interfaces (nucleation) and migration of interfaces (growth). The nucleation consists of the formation of a grain boundary due to dislocation generation, simultaneous recovery and rearrangement. This interface will become a nucleus for DRX when it attains a critical configuration, that of a large-angle boundary. The nucleus will grow by the process of grain boundary migration. Under hot working conditions the material acts essentially as a dissipator of power (negligible energy storage). The driving force for the migration of interfaces is therefore the reduction of total interface energy. When nucleation and growth occur simultaneously, the slower of these two will be controlling DRX.

Earlier this model was used for α-brasses [7] and it was shown that the DRX in α-brass is controlled by the rate of nucleation of interfaces which depends on the process of thermal recovery by climb, and hence diffusion plays an important role. The equation for the rate of interface formation was given as

$$R_F = \dot{\varepsilon} P_R / \mathbf{b}l \quad (5)$$

where $\dot{\varepsilon}$ is the strain rate, P_R the probability of recovery by climb given by $P_R = \exp(-Q_D/RT)$, **b** the Burgers vector, l the dislocation link length, R the gas constant and T the DRX temperature.

The equation for the rate of interface migration was given as

$$R_M = cD\Gamma/kT\mathbf{b} \quad (6)$$

where c = constant (10^{-6} m^{-1}), D is the diffusion coefficient, Γ the interface energy, k the Boltzmann constant and T the DRX temperature.

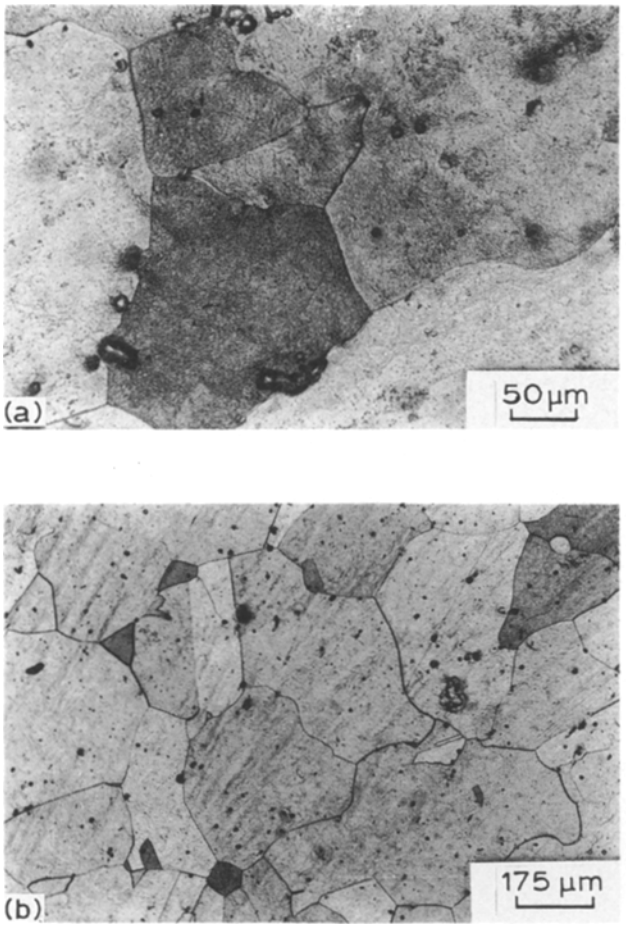

Figure 5 (a) Initial microstructure of α-nickel silver and (b) microstructure of specimen deformed at 950 °C and 0.01 s^{-1}, showing wavy boundaries.

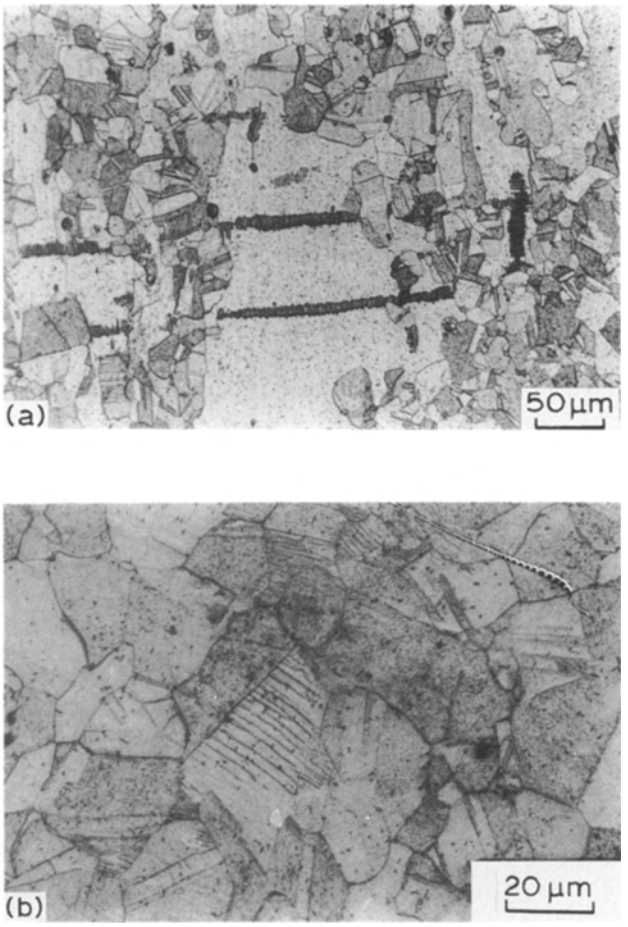

Figure 6 Microstructure of α-nickel silver specimen deformed at 700 °C and 10 s^{-1} (instability region) revealing (a) adiabatic shear bands and (b) strain markings.

Using the available data of the activation energy for diffusion [9], the rates of interface formation and migration are calculated: $R_F = 9.8 \times 10^5\ m^{-2}\ s^{-1}$ ($Q = 190\ kJ\ mol^{-1}$, $T = 1223\ K$, $\dot{\varepsilon} = 0.1\ s^{-1}$ and $\mathbf{b} = 2.6 \times 10^{-10}\ m$) and $R_M = 4.1 \times 10^{10}\ m^{-2}\ s^{-1}$ ($D = 9.2 \times 10^{-13}\ m^2\ s^{-1}$, $\Gamma = 200\ mJ\ m^{-2}$ (assumed)).

It is seen that the rate of interface formation is less than the rate of interface migration. Therefore DRX in α-nickel silver is controlled by the rate of interface formation which in turn is controlled by the diffusion-dependent climb.

As the DRX efficiency is dependent on the probability of climb which is controlled by diffusion, an increase in Q_D with the addition of nickel to Cu–Zn alloy decreases the probability of recovery and results in a drop in the efficiency of power dissipation. Due to the increase in Q_D, P_R in Equation 5 decreases. In order to compensate for the drop in the value of P_R, the strain rate for DRX nucleation increases in the case of α-nickel silver.

5.3. Instabilities at high strain rates

The instability criterion given by Equation 4 predicts that instabilities occur at high strain rates (10 and 100 s^{-1}). The stress–strain curves for specimens deformed under these conditions have peculiar shapes (Fig. 1). Microstructural investigations of specimens in the instability regime (Fig. 6) have shown that the manifestations are in the form of adiabatic shear bands (Fig. 6a) and strain markings (Fig. 6b). These disappear in the specimens deformed under the conditions below those of curve H in Fig. 3.

6. Conclusions

The hot deformation behaviour of α-nickel silver is studied in the temperature range 700–950 °C and strain-rate range 0.001–100 s^{-1}. The following conclusions are drawn from this investigation:

1. α-nickel silver exhibits a domain of dynamic recrystallization at temperature greater than 750 °C and at strain rates lower than 1 s^{-1}.
2. The maximum efficiency of power dissipation in the domain is 38% and occurs at about 950 °C and at a strain rate of 0.1 s^{-1}.
3. On the basis of a simple model, it is shown that the DRX in α-nickel silver is controlled by the rate of nucleation of interfaces which depends on the process of thermal recovery by climb, and hence diffusion plays an important role.
4. The material undergoes microstructural instabilities at high strain rates (10 and 100 s^{-1}) as predicted by the instability criterion. The manifestations are in the form of adiabatic shear bands and strain markings.

References

1. K. J. GARDNER and R. GRINES, *Met. Sci.* **13** (1979) 216.
2. D. N. CROWTHER and B. MINTZ, *Mater. Sci. Technol.* **2** (1986) 771.
3. P. J. WRAY, *Metall. Trans. A* **15A** (1984) 2009.
4. H. J. McQUEEN and J. J. JONAS, in "Treatise on Materials Science and Technology", Vol. 6 edited by R. J. Arsenault, (Academic Press, New York, 1975) p. 393.
5. O. D. SHERBY and P. M. BURKE, *Progr. Mater. Sci.* **13** (1968) 323.
6. J. HENNAUT, J. OTHMEZOURI and J. CHARLIES, *Z. Metallkde* **73** (1982) 744.
7. D. PADMAVARDHANI and Y. V. R. K. PRASAD, *Mater. Sci. Engg. A.* **157** (1992) 43.
8. D. M. WARD and B. J. HELLIWELL, *J. Inst. Metals* **98** (1970) 199.
9. K. J. ANUSAVICE and R. T. DeHOFF, *Metall. Trans. A* **3A** (1972) 1279.
10. D. PADMAVARDHANI and Y. V. R. K. PRASAD, *ibid.* **22A** (1991) 2996.
11. Y. V. R. K. PRASAD, H. L. GEGEL, S. M. DORAIVELU, J. C. MALAS, J. T. MORGAN, K. A. LARK and D. R. BARKER, *ibid.* **15A** (1984) 1883.
12. H. L. GEGEL, J. C. MALAS, S. M. DORAIVELU and V. A. SHENDE, in "Metals Handbook", 9th Edn. Vol. 14 (ASM International, Metals Park, Ohio, 1987) p. 417.
13. J. M. ALEXANDER, in "Modelling of Hot Deformation of Steels", edited by J. G. Lenard (Springer, Berlin, 1989) p. 101.
14. J. K. CHAKRAVARTTY, Y. V. R. K. PRASAD and M. K. ASUNDI, *Metall. Trans. A* **22A** (1991) 1089.
15. N. RAVICHANDRAN and Y. V. R. K. PRASAD, *ibid.* **22A** (1991) 2339.
16. D. PADMAVARDHANI and Y. V. R. K. PRASAD, *ibid.* **22A** (1991) 2985.
17. R. J. JACKSON, D. A. EDGE and D. C. MOORE, *J. Inst. Metals* **98** (1970) 193.
18. R. RAJ, *Metall. Trans. A* **12A** (1981) 1089.
19. A. K. S. KALYAN KUMAR, "Criteria For Predicting Metallurgical Instabilities in Processing, MSc thesis, Indian Institute of Science, Bangalore (1987).
20. Y. V. R. K. PRASAD, *Indian J. Tech.* **28** (1990) 435.
21. H. ZIEGLER, in "Progress in Solid Mechanics", edited by I. N. Sneddon and R. Hill (North-Holland, Amsterdam, 1963) p. 93.
22. D. PADMAVARDHANI and Y. V. R. K. PRASAD, *Z. Metallkde*, **84** (1993) 1.
23. W. ROBERTS, in "Deformation Processing and Structure", edited by G. Krauss (ASM, Metals Park, Ohio, 1984) p. 109.
24. N. RAVICHANDRAN and Y. V. R. K. PRASAD, *Bull. Mater. Sci.* **14** (1991) 1241.

Received 25 March 1992
and accepted 24 February 1993